Generation of super-resolution gap-free ocean colour satellite products using DINEOF.

Aida Alvera-Azcárate[1], Dimitry Van der Zande[2], Alexander Barth[1], Antoine Dille[2], Joppe Massant[2], and Jean-Marie Beckers[1]

[1]AGO-GHER, University of Liège, Allée du Six Aout, 17, Sart Tilman, Liège 4000, Belgium
[2]Royal Belgian Institute of Natural Sciences (RBINS), Direction Natural Environment Rue Vautier 29, 1000 Brussels, Belgium

Correspondence: Aida Alvera-Azcárate (a.alvera@uliege.be)

Abstract. In this work we present a super-resolution approach to derive high spatial and temporal resolution ocean colour satellite datasets. The technique is based on DINEOF (Data Interpolating Empirircal Orthogonal Functions), a data-driven method that uses the spatio-temporal coherence of the analysed datasets to infer missing information. DINEOF is used here to effectively increase the spatial resolution of satellite data, and is applied to a combination of Sentinel-2 and Sentinel-3 datasets. The results show that DINEOF is able to infer the spatial variability observed in the Sentinel-2 data into the Sentinel-3 data, while reconstructing missing information due to clouds and reducing the amount of noise in the initial dataset. In order to achieve this, both Sentinel-2 and Sentinel-3 datasets have undergo the same preprocessing, including a comprehensive, region-independent, and pixel-based automatic switching scheme for choosing the most appropriate atmospheric correction and ocean colour algorithm to derive the in-water products. The super-resolution DINEOF has been applied to two different variables (turbidity and chlorophyll) and two different domains (Belgian coastal zone and the whole North Sea), and the submesoscale variability of the turbidity along the Belgian coastal zone has been studied.

1   Introduction

The coastal ocean is a very dynamic region, both in space and time. Coastal regions are subject to strong anthropogenic pressure, and satellite data provide the necessary spatial and temporal coverage to study and monitor these regions. There is a need however to measure these areas at both high spatial and temporal resolution, in order to capture the relevant scales of variability. While "traditional" ocean colour satellites like Sentinel-3 provide daily temporal resolution, the sensors onboard these satellites do not measure at the necessary high spatial resolution to resolve complex coastal dynamics. High spatial resolution sensors, like the MultiSpectral Instrument (MSI) onboard Sentinel-2 (10 m - 60 m resolution), are able to resolve these small scales, but their temporal revisit time is far from optimal (about 5 days considering the Sentinel-2 A and B tandem). Additionally, both high spatial resolution datasets and traditional ones are hindered by the presence of clouds, resulting in a large amount of missing data.

Super-resolution approaches that are aimed at increasing the spatial resolution of geophysical datasets have been developed using neural network methodologies. For example, Thiria et al. (2023) used a convolutional neural network for increasing the spatial resolution of simulated geostrophic ocean currents, helped by simulated sea surface temperature data. Liu and Wang (2021) also used convolutional neural networks, this time for increasing the spatial resolution of low-resolution bands on-board the VIIRS (Visible Infrared Imaging Radiometer Suite) sensor, in order to obtain high spatial resolution ocean colour products. Kim et al. (2023) and Lambhate and Subramani (2020) increased the spatial resolution of sea surface temperature data using Generative Adversarial Networks, and Zou et al. (2023) used a transformer model also with sea surface temperature. Barthélémy et al. (2022) used a super-resolution data assimilation approach, based on an enhanced deep super-resolution network, to ingest high spatial resolution observations into a hydrodynamical model. Peach et al. (2023) compared process-based and data-driven approaches based on neural networks to increase the spatial resolution of wave forecasts, and Buongiorno Nardelli et al. (2022) used a deep convolutional neural network to infer high spatial resolution ocean dynamics from satellite data. Applications are very diverse in terms of used methodologies and variables. In this work, we are proposing a data-driven approach based on DINEOF (Data Interpolating Empirical Orthogonal Functions, Beckers and Rixen (2003); Alvera-Azcárate et al. (2005)) to increase the spatial resolution of Sentinel-3 ocean colour data using Sentinel-2 data. The aim is to obtain a unique dataset with the temporal resolution of Sentinel-3 and the spatial resolution from Sentinel-2, by combining both data streams. DINEOF was developed to interpolate missing data due to *e.g.* the presence of clouds, but as it will be shown here it can also, at the same time, increase the resolution of the final, cloud-free dataset. DINEOF uses a truncated EOF basis to infer missing information in satellite datasets hindered by the presence of clouds. The EOF basis extracts the dominant spatio-temporal variability and is therefore an efficient approach to extract high spatial variability. As a data-driven technique, it is entirely based on the available data, and does not need any a priori information about scales of variability or signal-to-noise ratio, or other input variables, which makes its use easy and adaptable to any geophysical variable.

A huge challenge when working with several datasets to obtain a unique estimate of an ocean variable is the heterogeneity of the different sources: differences in the spectral bands present in each satellite (Blondeau-Patissier et al., 2014; Groom et al., 2019), different spatial resolutions, and also a difference in the measurement time. This last factor can result in large differences in dynamic regions, as is the case of the North Sea. In these regions, variables like chlorophyll-a concentration or turbidity can experience large changes within a few hours due to the influence of strong tidal currents, storms and the wave field (Fettweis et al., 2010; Wilson and Heath, 2019; Desmit et al., 2024), an influence that is, in addition, dependent on the bathymetry. The region of study, the Belgian coast in the North Sea (figure 1), is a shallow region characterized by a series of sandbanks and dredging channels that influence water dynamics and bottom sediment resuspension. In this work, we aim at minimising the differences due to the spectral characteristics of the Sentinel-2 and Sentinel-3, as it will be explained in section 2. The difference in time does not pose a problem in this study, since for a given day only one data source is used (Sentinel-2 if present or Sentinel-3 otherwise), and no merging of the two satellite datasets is performed.
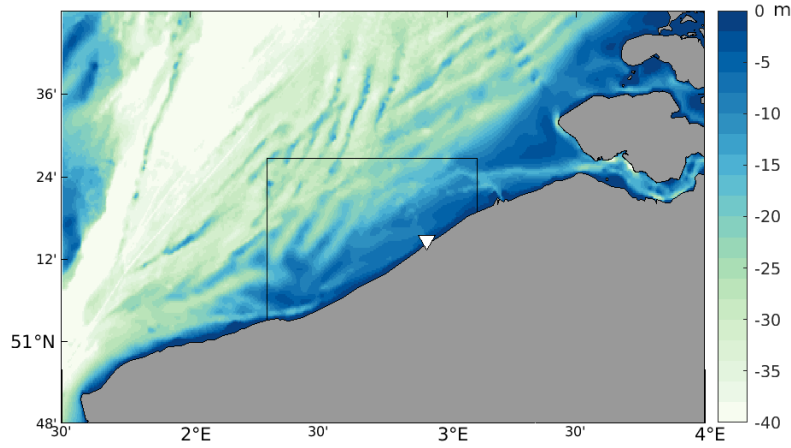
Figure 1. Bathymetry (m) of the southern North Sea. The black square shows the region used in this study and the white triangle shows the position of the validation station, RT1.

This work is organized as follows: section 2 describes the region of study, the satellite data and the in-situ data used. This section is followed by a description of the methodology to produce super-resolution data using DINEOF (section 3). The results, including the validation and an assessment of the scales resolved by all data sources, are presented in section 4. A description of small-scale variability in the southern North Sea using the super-resolution dataset is presented in section 5, and we conclude this work in section 6.

2 Data used

2.1 Study Area

This study focuses on dynamics and optically complex waters in the Belgian Coastal Zone (BCZ). The BCZ is a relatively shallow (<50 m) well-mixed shelf sea, connected to the North Sea in the north and to the English Channel in the west (Ruddick and Lacroix, 2006). It is characterized by a relatively high suspended sediment concentration, with a gradient from several hundreds of g/m^3 nearshore to $< 1 g/m^3$ in the offshore waters, inversely related to the bathymetry (Nechad et al., 2009, 2011; Neukermans et al., 2012). Strong tidal currents and the tidal resuspension of sediments is the main cause of the high turbidity in the nearshore area (Fettweis and Van den Eynde, 2003; Fettweis et al., 2007). Annually recurring phytoplankton blooms are observed in spring and summer. These blooms are generally composed of diatoms and Phaeocystis globose (Lacroix et al., 2007). In recent years, blooms have been occurring earlier, likely in response to sea surface temperature increases and changes in nutrient outputs (Desmit et al., 2020; Alvera-Azcárate et al., 2021b). The water type is turbid coastal to turbid coastal with

75 high organic content. The water at the Research Tower 1 (RT1) near Oostende (51.24643°N, 2.91933°E), used in the validation of the various datasets in this work, is turbid with tidal variability and with an occasional outflow from the port of Oostende (Belgium) reaching the site.

2.2 Satellite data

80 The ocean colour satellite products used in this study are generated following the methodology applied in the Copernicus Marine high-resolution service using a multi-algorithm approach which aims at combining the best suited algorithm for different water types. The year 2020 has been chosen for the test period, as this year has the largest unbroken timeseries of independent in situ data at the Oostende RT1 station, used to validate the super-resolution DINEOF product and its potential in capturing the coastal turbidity dynamics. To facilitate Sentinel-2 and Sentinel-3 product generation, the processor is fully automated

85 and set up in the DIAS cloud environment CREODIAS (https://creodias.eu/). This processor starts from L1C and L1 data for Sentinel-2/MSI and Sentinel-3/OLCI respectively and combines atmospheric correction processing (C2RCC + ACOLITE Dark Spectrum Fitting), IDEPIX pixel classification, ocean colour algorithm application and product quality control (e.g. glint flagging, bottom reflection flagging, etc.) to provide Analysis Ready Data Layers (ARDL), i.e. chlorophyll (CHL), turbidity (TUR) and suspended particulate matter (SPM). A schematic overview of the different processing steps taken is provided in

90 figure 2.

2.2.1 Remote sensing reflectance and pixel classification

In order to obtain high-quality remote sensing reflectance (RRS) spectra for a large number of pixels while maintaining the ability to handle both atypical water conditions and challenging atmospheric conditions, the atmospheric correction algorithms

95 ACOLITE-DSF (https://github.com/acolite/acolite) and C2RCC (https://c2rcc.org/) are combined to process L1C products to L2R (Level 2 RRS products). While both algorithms have their strengths and weaknesses, they each use different approaches to estimate RRS. C2RCC uses an underlying water reflectance model to fit the estimated RRS spectrum to a known form within the boundaries of the training dataset. This method reduces noise in low RRS situations and provides greater retrieval power in difficult circumstances, such as sun glinted and highly absorbing waters. On the other hand, ACOLITE-DSF does not assume

100 a specific water reflectance model, allowing it to return unusual Rrs spectra that correspond to optical properties not found in typical water reflectance models. This can complement C2RCC where it is less performant, such as dredging plumes and unusual algae blooms.

To combine the two approaches, a comprehensive, region-independent, and pixel-based automatic switching scheme is re-

105 quired, along with a technique for achieving a seamless transition between the two algorithms. The C2RCC to ACOLITE/DSF pixel-based switching is performed by means of band comparison of the RRS560 and RRS865 products (defined as green-nir -near infrared- ratio) as provided by the C2RCC processor. The green-nir ratio can be modelled using a logarithmic regression
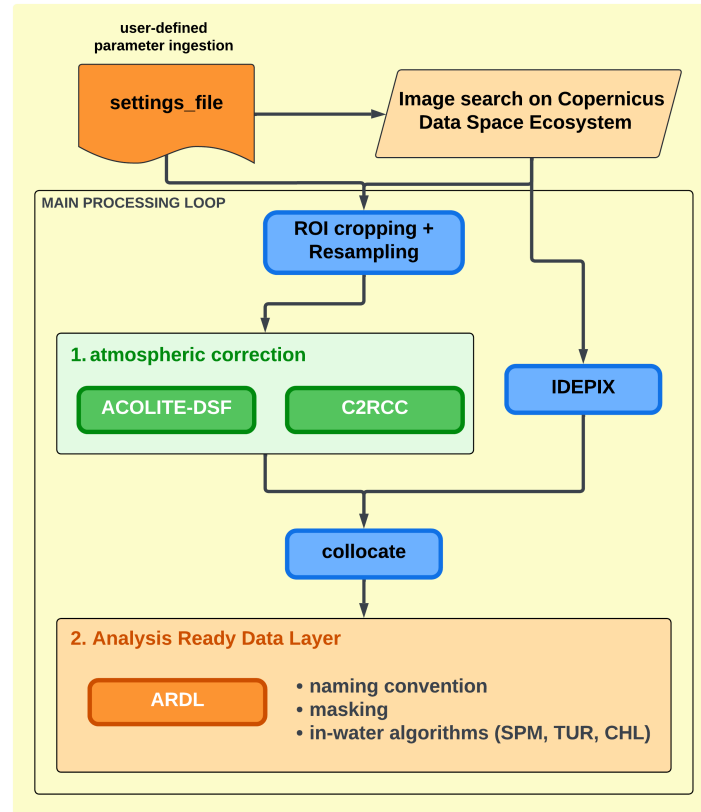
Figure 2. Processing steps applied for deriving L2 ARDL products, used for both the Sentinel-2/MSI and Sentinel-3/OLCI sensors. The processor combines the atmospheric correction algorithms ACOLITE and C2RCC, uses SNAP to crop and resample the data to the Region of Interest, runs IDEPIX for pixel classification after which all the intermediate layers are collocated together to the required resolution. In the final step, the in water ocean colour products are generated using specialized algorithms.

curve which starts as linear for the smaller reflectance values, but bends at the point where the saturation of the most sensitive band (i.e. RRS560) occurs. C2RCC pixels which deviate from the logarithmic model are considered erroneous outputs. The

110 ACOLITE/DSF processor has the ability to provide higher RRS ranges compared to C2RCC while being noisier for lower RRS values thus highlighting the complementary between the two approaches. The green-nir ratio value of 45 is selected as the transition point between C2RCC and ACOLITE/DSF products. To ensure a smooth transition between the different atmospheric corrections, a weighted transition is applied between the green-nir ratio boundaries of 50 and 40 based on the method described by Novoa et al. (2017). The C2RCC to ACOLITE/DSF pixel-based switching is described in detail in Van der Zande

115 et al. (2023). Compatibility between the Sentinel-2/MSI products and the Sentinel-3/OLCI products was ensured by applying the identical processing chain to both datasets.
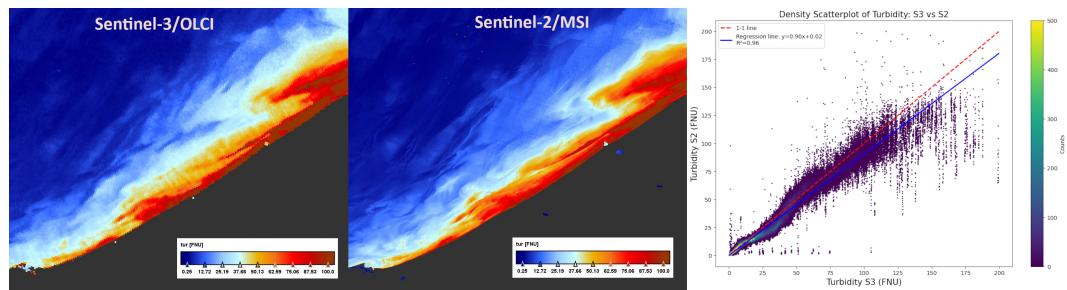
Figure 3. TUR products for 5 April 2020 for the Belgian Coastal Zone region generated using the multi-sensor processor using Sentinel-3/OLCI (left) and Sentinel-2/MSI (middle) source data. The right panel shows a density scatter plot of the Sentinel-3 versus Sentinel-2 datasets.

The IDEPIX software (v2.2.10, algorithm update 8.0.3), available as a SNAP (Sentinel Application Platform) processor, is used for pixel classification, including cloud masking, cloud shadow identification, sea ice, floating vegetation, sub-pixel objects (ships, small islands and rocks), and the land-water distinction taking temporary water bodies (e.g. intertidal areas, lagoons) into account. SNAP is a software developed by the European Space Agency (ESA) designed for processing and analysing Earth observation data, particularly from the Sentinel satellites. It provides a common architecture for all Sentinel Toolboxes and enables the application of the C2RCC and IDEPIX processor on both Sentinel-2 and Sentinel-3 images.

2.2.2 Turbidity and Suspended Particulate Matter

The SPM and the TUR products were generated using the generic multi-sensor algorithm described by Nechad et al. (2010). This algorithm provides the theoretical basis for SPM and TUR as a function of reflectance (RRS) at a single band, and provided calibration coefficients for all wavelengths, between 520 nm and 885 nm. It defines a relationship where RRS increases monotonically with SPM/TUR, at first linearly and then tends towards an asymptotic or "saturation" reflectance. This means that RRS becomes insensitive to changes in SPM/TUR which has led to the development of "switching single band algorithms" (Novoa et al., 2017) using using different wavelengths at different SPM concentrations to avoid the saturation effect and typically a smooth weighting between two adjacent spectral bands to avoid image artefacts. The Novoa et al. (2017) approach is applied to both the SPMand TUR products providing a multi-band SPM and TUR product using two bands (red: 665 nm and near-infrared: 865 nm). An example of the TUR products for the Belgian Coastal Zone region is provided in figure 3 showing a good correspondence between both the Sentinel-2/MSI and Sentinel-3/OLCI products providing information at different spatial and temporal resolutions. The Sentinel-2 and Sentinel-3 data have been interpolated to the same 60 m resolution grid, as both data need to be on the same grid as it will be explained in section 3.

2.2.3 Multi-sensor chlorophyll data

140 In order to assess the small-scale information retained in the final DINEOF reconstructions, an additional test on a larger region has been done, using data at 1 km resolution. The aim is to create a degraded 5 km resolution dataset from the initial data and to compare the DINEOF results to the initial, non-degraded dataset. This scale assessment is described in section 4.3. Daily chlorophyll data at a spatial resolution of 1 km, obtained from the level-3 multi-sensor cmems_obs-oc_atl_bgc-plankton_my_l3-multi-1km_P1D product from CMEMS (Copernicus Marine Service, https://doi.org/10.48670/moi-00286),

145 are used in this analysis. This product includes data from different sensors (SeaWIFS, MERIS, MODIS-Aqua, MODIS-Terra, VIIRS-SNPP, VIIRS-JPPS1, OLCI-S3A and OLCI-S3B) and covers the whole North Sea area (48.46°N - 55.96°N; -1.64°E - 6.15°E). We have extracted data from 1 February 2022 to 1 November 2022 in order to have a long time series of data, avoiding January and December which have low-light conditions and prevent the calculation of ocean colour variables at the higher latitudes of the domain. The choice of the year was simply to avoid 2020 which is used in the other tests. A total of 271

150 images are available, with an average amount of missing data, due to cloud cover and quality control, of 38.17%.

2.3 In situ data

The RRS products were validated using Pan-and-Tilt Hyperspectral Radiometer system (PANTHYR, Vanhellemont (2020); Vansteenwegen et al. (2019)) for the period 2019-2022. An autonomous PANTHYR system has been deployed at the Research

155 Tower 1 (RT1) near Oostende (RT1, 51.24643°N, 2.91933°E). The PANTHYR system has two TriOS RAMSES radiometers mounted on a pan-and-tilt head, one for up- and downwelling spectral radiances, and one with a cosine collector to measure spectral irradiance, enabling to determine the RRS signal. The PANTHYR measures autonomously every 20 min at programmed relative azimuth angles to the sun. In the present study, measurements were made at a 270° azimuth angle. Because of the hyperspectral measurements, one significant advantage of the PANTHYR datasets when compared to AERONET-OC,

160 typically used for validating ocean-colour satellites (Zibordi et al., 2009), is that the hyperspectral instrument permits the validation of all MSI and OLCI VNIR bands within the 400-900 nm range, including several nearinfrared (NIR) bands not available with the AERONET-OC instrument. RRS data were finally convolved to the relative spectral response functions of the MSI and OLCI instruments on Sentinel-3 A and B and Sentinel-2 A and B.

165 Matchups for PANTHYR stations were extracted from shifted locations near the deployment tower, to avoid platform effects such as direct pixel contamination and shadows, as well as in-water wakes. For the match-up extraction, a maximum time difference of 2 hours between in situ observation and satellite overpass was allowed. However, the high frequency measurement protocol from the in-situ measurement stations resulted in shorter time differences between in situ and satellite observations. The matchup validation protocol described by Bailey and Werdell (2006) was applied to remove erroneous matchups from the

170 analysis. Macro-pixels of 15x15 60 m pixels for Sentinel-2/MSI and 3x3 300 m for Sentinel-3/OLCI were extracted from the L2 products. This box allows for the evaluation of spatial stability, or homogeneity, at the validation point. For the satellite

data it was required that at least 60% of the pixels in the defined box be valid (*i.e.* unflagged) to ensure statistical confidence in the mean values retrieved. The arithmetic mean and standard deviation of the non-masked pixels was determined enabling the computation of the coefficient of variation (standard deviation divided by the filtered mean). Satellite retrievals with extreme variation between pixels in the defined box (coefficient of variation > 0.15) were excluded from the matchup analysis.

3   Methodology

3.1   DINEOF

DINEOF (Data Interpolating Empirical Orthogonal Functions, Beckers and Rixen (2003); Alvera-Azcárate et al. (2005)) is used to calculate the reconstruction of the data and to enhance the resolution of the combined Sentinel-2 and Sentinel-3 dataset. DINEOF computes the missing data information from a three-dimensional dataset by calculating a truncated Empirical Orthogonal Function (EOF) basis. These EOFs are calculated increasingly (starting from one until the optimal number of EOFs is found) and iteratively until a convergence is reached, and at each iteration the estimate of the missing data is updated using the latest EOF modes. About 3% of valid data (in the form of clouds, following Beckers et al. (2006)) is masked at the beginning of the procedure, and these data are used to determine the number of EOFs that minimizes the reconstruction error (in terms of its Root Mean Square Error, RMSE). When three consecutive EOFs provide an increasingly higher RMSE, the procedure is stopped and the final reconstruction is performed with the optimal amount of EOFs determined by this cross-validation.

In addition to the reconstruction of missing data in several variables (*e.g.* sea surface temperature (Alvera-Azcárate et al., 2005), chlorophyll (Alvera-Azcárate et al., 2021b), turbidity (Alvera-Azcárate et al., 2015), salinity (Alvera-Azcárate et al., 2016) as well as multivariate reconstructions (Alvera-Azcárate et al., 2007)), DINEOF has been used to detect outliers in satellite data (Alvera-Azcárate et al., 2012, 2015) and shadows in high spatial resolution satellite data (Alvera-Azcárate et al., 2021a). DINEOF has therefore shown it can perform a wide range of analysis of satellite data with the aim of improving their quality and completeness.

3.2   Generation of super-resolution data

In order to obtain a super-resolution reconstruction from the combination of Sentinel-3/OLCI and Sentinel-2/MSI data mentioned in section 2, the initial gappy matrix is prepared as follows: Sentinel-2 data are used on days when they are available, and on days with no Sentinel-2 coverage, Sentinel-3 data, interpolated at the Sentinel-2 spatial resolution, are used. The matrix consists therefore of a mixture of Sentinel-2 and Sentinel-3 data. The interpolation of Sentinel-3 data onto the Sentinel-2 grid is done to preserve the size of the matrix, which has to be constant in order to be used in DINEOF, and also to determine the

spatial resolution of the final dataset, but no gain in resolution is done at this step.

On days when both Sentinel-2 and Sentinel-3 data are available, only Sentinel-2 data are used. We could slightly increase the spatial coverage on these days by combining both datastreams but we had found the increase to be very small, since cloud distribution does not change substantially between the Sentinel-3 and Sentinel-2 passes. In addition, depending on the tidal currents, the difference in turbidity between the two satellite passes can be quite high, and this can lead to discontinuities between both estimates, which in turn can be retained in the final dataset. We have decided therefore to avoid this problem by using a unique data source on a given day.

The initial dataset with the combined Sentinel-2 and Sentinel-3 data has 210 time steps, of which 63% are Sentinel-3 data and 37% are Sentinel-2 data. Days with too high cloud coverage (more than 98% of missing data over the study region) are not used, which brings the final size to 163 days, distributed from 18 January to 17 December 2020.

The combined dataset is fed to DINEOF as a unique matrix. As DINEOF performs all calculations on the initial grid, it is important that the initial data are already interpolated to the final grid that we want to obtain (i.e. the high spatial resolution grid). Through the EOF basis calculation, the high spatial information of Sentinel-2 is extracted by the EOFs, and this information is then projected into the final dataset by the EOF basis, effectively increasing the spatial resolution of the initial dataset.

4   Results

4.1   Super-resolution data

Super-resolution DINEOF (section 3) has been applied to the turbidity data in the Oostende region described in section 2. The initial matrix has 45% of missing data. DINEOF has been applied to the combined Sentinel-2 and Sentinel-3 data for 2020 and 23 EOFs were retained as optimal for the reconstruction, with a cross-validation error of 1.4 FNU. The size of the matrix was $946 \times 789 \times 210$ (longitude, latitude and time), and the DINEOF run took 8 hours to complete (on an Intel Core i9-10900X CPU at 3.70GHz). The only two optional parameters to set in DINEOF are related to the filtering of the temporal covariance matrix (Alvera-Azcárate et al., 2009) and were fixed to $\alpha = 0.01$ (the amplitude of the filter) and $n = 3$ (the number of iterations of the filter). These result in a filter of about 1.1 days. As shown in Alvera-Azcárate et al. (2009), the use of this filter can result in more EOFs being retained as optimal, which in turn results in a higher variability in the final results. Several tests were performed for values $\alpha = 0.01$ to $\alpha = 0.1$ and $n = 1$ to $n = 10$ and the combination that maximized the number of EOFs was retained. The first three EOFs explain, respectively, 59.04%, 25.73% and 3.74% of the total variability of the dataset, and the 23 EOFs retained explain a total of 97.9% of the variability. When analysing the spatial and temporal structure of these EOFs, we can observe the influence of small scale variability contained in them. The first EOF mode (figure 4) displays an inshore-offshore gradient, in which more turbid waters are found in the nearshore region. An increasing turbidity along the
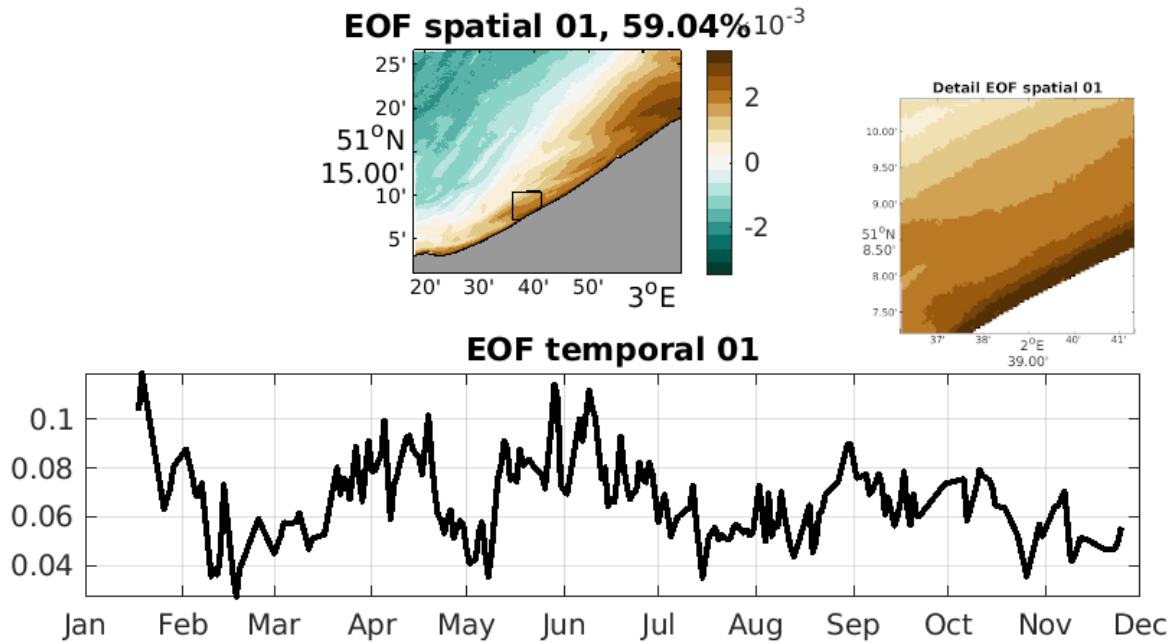
Figure 4. First EOF mode of the 2020 turbidity data obtained by DINEOF. Top left: spatial EOF mode. Top right: detail of the spatial mode on the black square shown in the left panel. Bottom: temporal EOF mode.

coast is found towards the region of the Scheldt river estuary. The factors responsible for higher turbidity in this region have been attributed to tides and meteorological conditions (Fettweis and Van den Eynde, 2003), and show peaks in January, April, June and September-October 2020. This mode shows large-scale processes, and there is no apparent small-scale variability present in the first spatial EOF.

The second EOF mode (not shown) already displays small-scale spatial variability. We show here the third EOF mode (figure 5), which shows a northeast-southwest gradient, with high variability in the temporal mode. On the detail panel shown in the figure we can also appreciate a thin region along the coast with oposite behaviour than the more offshore waters. It has been shown (https://www.esa.int/Applications/Observing_the_Earth/Copernicus/Sentinel-2/Near-shore_phytoplankton_bloom_captured_from_space) that Sentinel-2 is able to capture small scale varibility that was previously unknown, thanks to its high spatial resolution, a variability that has been captured by the EOF basis to produce the final, super-resolution datasets that will be shown in this section. The validation of the initial data and the super-resolution reconstruction will be presented in section 4.2.

Figure 6 shows the initial turbidity data on 9 May 2020, a day with initially Sentinel-3 data (hence, low resolution data). A day with low cloud coverage has been chosen in order to show the capability of DINEOF to enhance the spatial resolution.
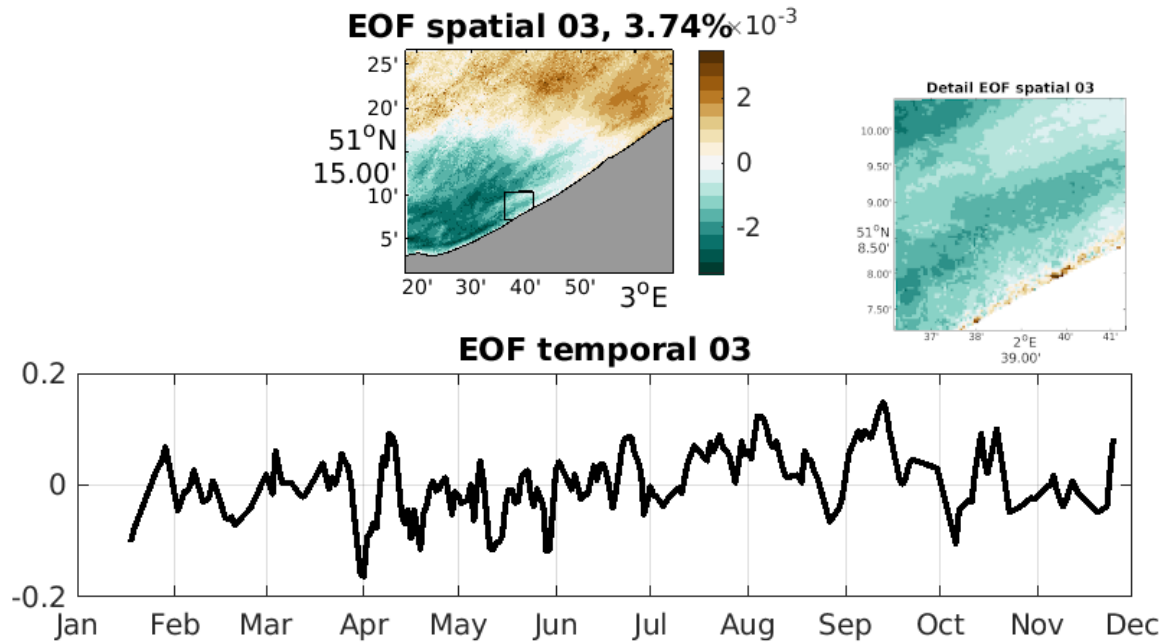
Figure 5. Third EOF mode of the 2020 turbidity data obtained by DINEOF. Top left: spatial EOF mode. Top right: detail of the spatial mode on the black square shown in the left panel. Bottom: temporal EOF mode.

The initial data (figure 6 top left panel) show a series of high and low turbidity regions, a pattern that is due to the presence of sandbanks close to the Belgian coast. The changes in depth in this region induce large differences in turbidity from day to day. High turbidity values in the east of the figure are due to the Scheldt-Rhine river plume, located to the east of the domain. The reconstructed image (figure 6 top right panel) reproduces all these features, as it is also seen in the contours added to this figures. A north-south transect is also included in the figure to show the small scale variability that has been included in the reconstruction. The initial data (in blue in the middle panel of figure 6) does not contain this small scale variability, and presents instead a step-like nature due to the low spatial resolution of the initial dataset. This step-like variability is absent from the final, super-resolution data, which instead shows smaller-scale variability. A percentage change map is also included, showing differences between the initial and final product over the whole domain, with a dominance of along-coast structures following the sandbanks present in the region and that cause changes in turbidity. Most of the changes between the initial and final product affect therefore the structure of these sandbanks and other high turbidity features offshore. The difference in resolution between the initial and final products is also responsible for the changes observed in this figure. Sentinel-2 data have a 60 m resolution, Sentinel-3 data are 300 m resolution, and the DINEOF reconstruction should be between these two. The sandbanks have different TUR intensities in all products, and since they presnet sharp gradients, this will be felt in the percentage change map.
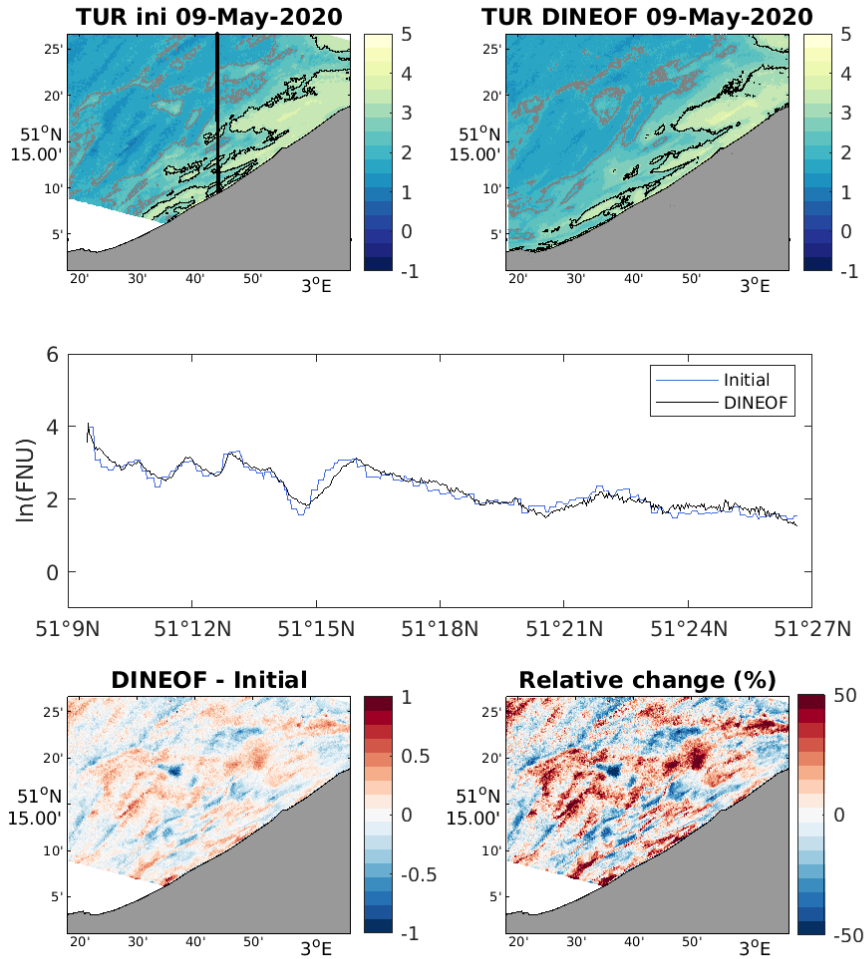
Figure 6. Top left: initially cloudy data at 300 m resolution, on 9 May 2020 (logarithmic scale, units ln(FNU)). Top right: DINEOF run of the mixed Sentinel-2 and Sentinel-3 dataset, at 60 m resolution (logarithmic scale). Grey contours in top panels: 1.5 ln(FNU), black contours: 3 ln(FNU). Middle panel: north-south transect for the two datasets (blue: initial data at 300 m; black: super-resolution DINEOF reconstruction). Bottom left: difference between initial and reconstructed data. Bottom right: percentage difference map.

Figure 7 shows a similar reconstruction as in figure 6, but this time for a date in which Sentinel-2 data are available (hence, high spatial resolution data). This example shows that the variability of the super-resolution DINEOF reconstruction is similar to the one of the initial dataset, and there is only a limited amount of variability lost with the analysis, mostly in regions with low values of turbidity (figure 7 middle panel). The presence of high turbidity regions caused by the presence of sandbanks is also visible in this image, and a strong inshore-offshore turbidity gradient can be seen, which is well retained by the re-

construction. The contours in both images show the small sclae variability retained in the reconstruction. Turbid waters in the eastermost part of the domain, close to the Scheldt estuary and the shallowest region of the domain, can also be seen. The percentage change map in this figure shows smaller-scale features, long and thin structures shown in an along-shore direction, showing that the turbidity around the sandbanks and also in offshore high turbidity features is being modified between the initial and final datasets. Again, the difference in resolution between the different initial products reflects in the representation of sharp turbidity gradients in the final product.

The results shown so far are from images that have good data coverage, but DINEOF also provides super-resolution data on days with high cloud coverage. Two examples are shown in the supplementary material, showing the reconstruction in a day with almost no initial data (figure 17) and a day with a high amount of noise in the initial data (figure 18). On days with almost no data (figure 17 on 12 April 2020), DINEOF is still able to provide a reconstruction with a good spatial variability. The reconstrution of the turbidity spatial distribution on days with high amounts of missing data is possible because of the three-dimensional nature of DINEOF, which exploits the spatio-temporal coherence of the data and enhances temporal correlations (Alvera-Azcárate et al., 2009).

At some moments, there can be outliers or noise in the initial dataset, despite the strong quality controls applied to the data, as in figure 18. The fact that DINEOF uses a truncated EOF basis to compute the missing data results in a partial loss of variability. However, this truncated EOF basis guarantees that the presence of outliers does not influence the overall quality of the reconstruction. As an example, in figure 18 we can see the turbidity on 28 May 2020, with a region in the northern part affected by the presence of noisy data. These are probably due to non-detected thin clouds. The north-south transect shows that the variability of these data far exceeds normal variability expected for the region. The DINEOF super-resolution results provide a reduced amount of noise and an improved quality of the final product, while still providing an accurate depiction of small scale variability.

4.2 Validation

Using the in-situ data described in section 2.3, a quality assessment of the initial data and the DINEOF results has been realised. Figure 8 shows the RRS matchups between Sentinel-2/MSI and the PANTHYR in situ instrument installed on RT1. The metrics used are described in the Appendix. In the considered deployment period between 2019-12-11 and 2023-08-01, 528 MSI L1C images were available for processing with 59 matchups with the PANTHYR instrument which passed the quality flagging of the individual atmospheric corrections (i.e. ACOLITE-DSF and C2RCC), IDEPIX quality flagging and the match-up quality flagging. When using the merged approach for atmospheric correction, the best performing bands are 490, 560, 665, and 704nm which are typically used for retrieval of turbidity and turbid water chlorophyll-a. For these bands the MAPE ranges between 9.88% and 17.20%.
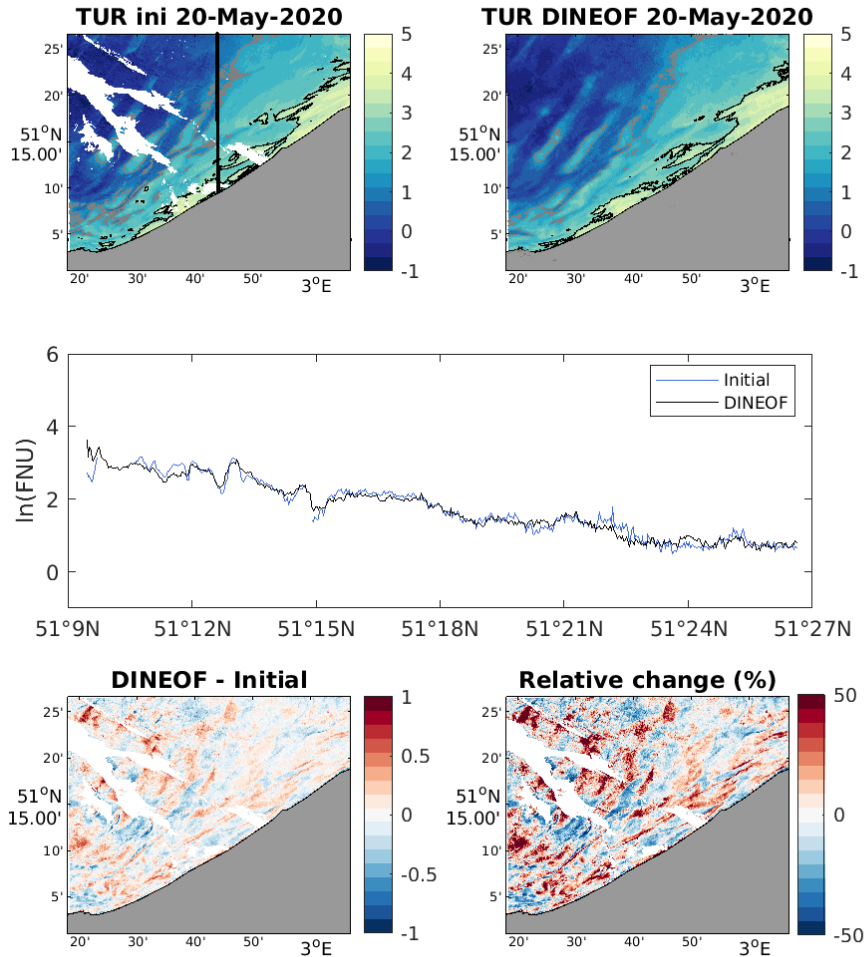
Figure 7. Top left: initially cloudy data at 60 m resolution, on 20 May 2020 (logarithmic scale, units ln(FNU)). Top right: DINEOF run of the mixed Sentinel-2 and Sentinel-3 dataset, at 60 m resolution (logarithmic scale). Grey contours in top panels: 2 ln(FNU), black contours: 3 ln(FNU). Middle panel: north-south transect for the two datasets (blue: initial data at 60 m; black: super-resolution DINEOF reconstruction). Bottom left: difference between initial and reconstructed data. Bottom right: percentage difference map.

Figure 9 shows the RRS matchups between the Sentinel-3/OLCI and the PANTHYR instrument installed on RT1. In the deployment period between 2019-12-11 and 2023-08-01, 2334 OLCI L1FR images were available for processing with 179 common matchups with the PANTHYR instrument which passed the quality flagging of the individual atmospheric corrections (i.e. ACOLITE-DSF and C2RCC), IDEPIX quality flagging and the match-up quality flagging. For the merged approach of
310   atmospheric correction, the best performing bands are 443, 490, 560, 665, and 709nm which are typically used for retrieval of

turbidity and turbid water chlorophyll-a. For these bands the MAPE ranges between 10.74% and 19.00%.

The accuracy of the DINEOF super-resolution products was validated for the Belgian Coastal Zone region by using the hyperspectral in situ data set from the autonomous PANTHYR systems deployed at Research Tower 1 (RT1) near Oostende to generate an in-situ turbidity product which was directly compared with the satellite derived turbidity products. The in-situ turbidity product was generated with the same algorithm as used for the satellite products. Figure 10 shows the turbidity time series for 2020 overlaying the in-situ data, both the Sentinel-2 and Sentinel-3 turbidity products and the final super-resolution DINEOF gap-filled product showing that the DINEOF product is able to capture the in situ turbidity signal between March and September. In January and February the DINEOF product shows slightly lower values which can be caused by the fact that in those months the availability of cloud-free satellite products from Sentinel-2 and Sentinel-3 is very scarce.

An objective intercomparison was achieved by a match-up analysis. For the match-up extraction, a maximum time difference of 1 hour between in situ observation and satellite overpass was allowed. The matchup validation protocol described by Bailey and Werdell (2006) was applied, to remove erroneous matchups from the analysis based on macro-pixels of 3x3 pixels from the satellite turbidity products. Figure 11 shows the results of the match-up analysis for Sentinel-2, Sentinel-3 and the gap-filled DINEOF super resolution products. These graphs show that both the Sentinel-2 and Sentinel-3 products show a good agreement with the in-situ observations with mean average percentage differences around 6%. The temporal frequency of Sentinel-3 overpasses over the region of interest results in more than 3 times more matchups. Considering the DINEOF super resolution matchups, this number of matchups is increased by another 34% with very similar statistics compared to the Sentinel-3 matchups, showing DINEOF's ability to retain the turbidity information provided by the source products. We do see a slight underestimation of the turbidity values by both satellites, especially for higher values (turbidity > 50 FNU). Further inspection indicates that this underestimated happens mostly in winter months (January-February), probably due to the high cloud cover (data not shown).

4.3 Scale Assessment

In order to determine which scales are reconstructed in the super-resolution DINEOF approach, a test using the multi-sensor satellite chlorophyll data at 1 km spatial resolution described in section 2.2.3 was performed. These data are downscaled to 5 km using a near neighbourgh interpolation (to avoid smoothing the data). Following the same procedure as with the combined Sentinel-2 and Sentinel-3 turbidity dataset, we intercalate the 1 km spatial resolution data and the 5 km spatial resolution data. The ratio of this mixed dataset is 1 high resolution image (at 1 km) for every 3 low resolution images (at 5 km), to mimic the ratio of the Sentinel-2 and Sentinel-3 combination used in the previous section. This allows us to compare the scales reconstructed on this dataset with the initial 1 km resolution data, both on days in which 1 km data and 5 km data were used. In addition, we have also made a reference reconstruction of the original, 1 km spatial resolution data, so that we can assess how
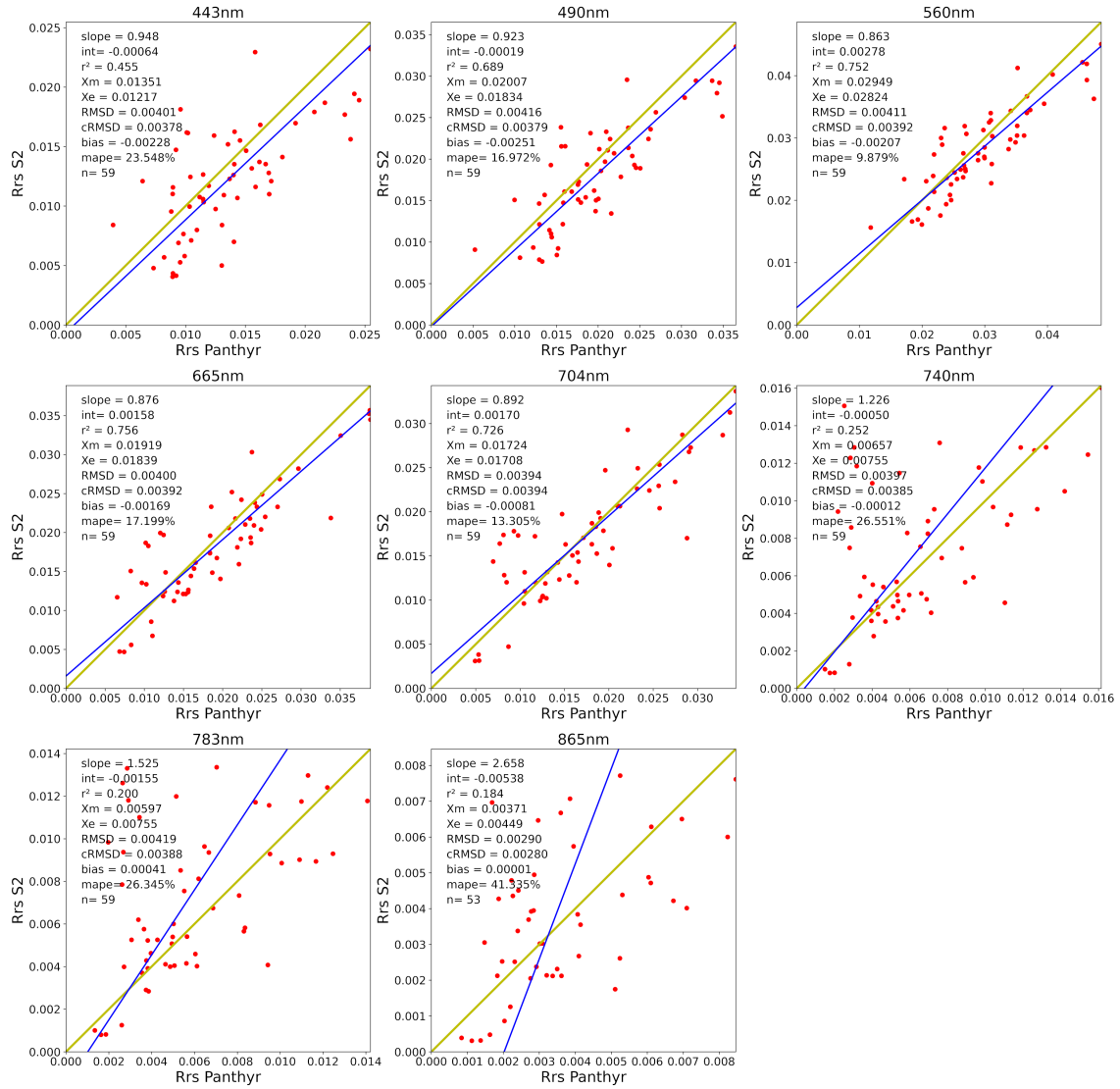
Figure 8. Validation of remote sensing reflectance (RRS) for Sentinel-2/MSI data. Hyper-spectral in situ stations from the HYPERNET network in Oostende (Belgium) were used.
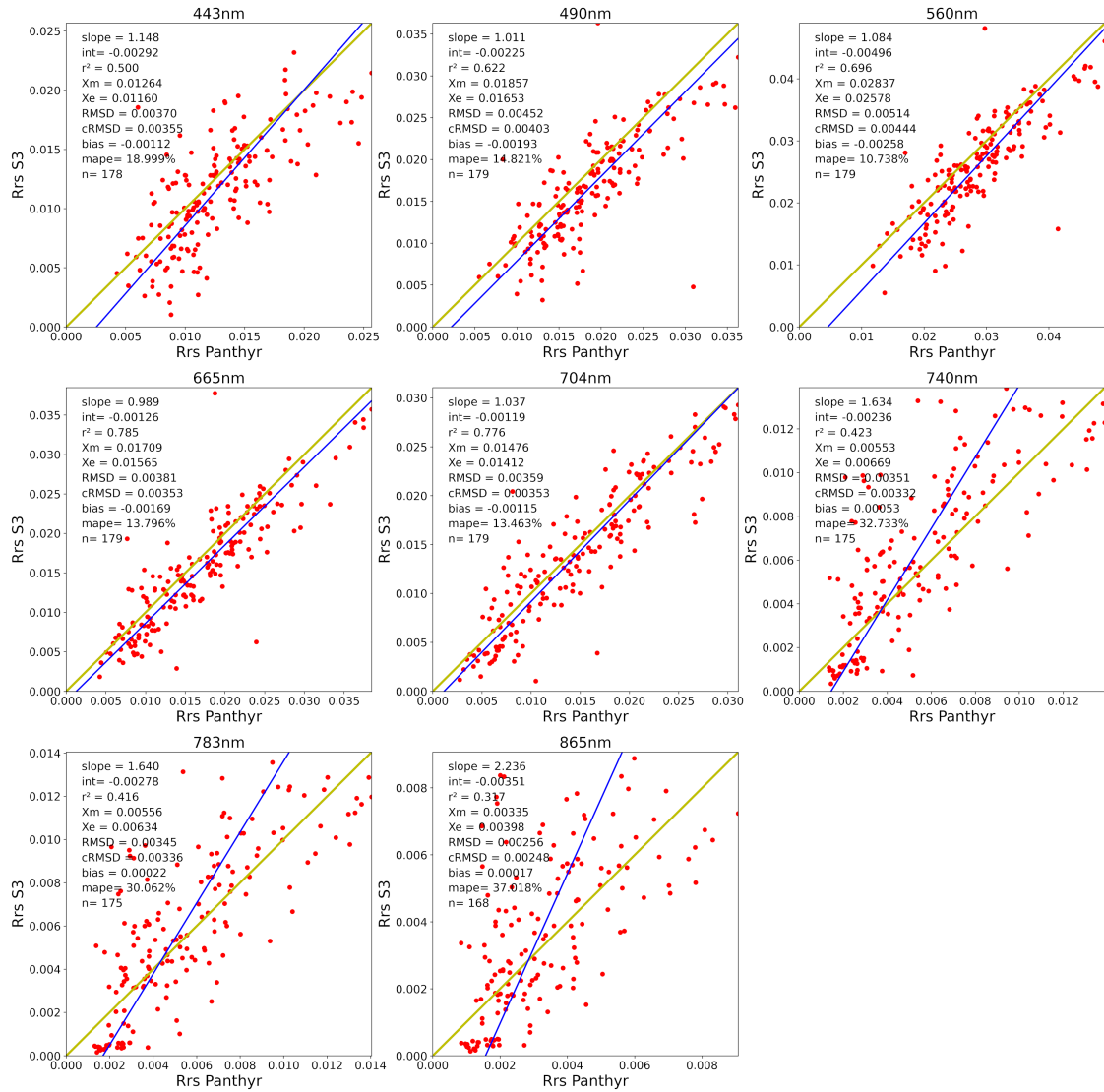
Figure 9. Validation of remote sensing reflectance (RRS) for Sentinel-3/OLCI data. Hyper-spectral in situ stations from the HYPERNET network in Oostende (Belgium) were used.
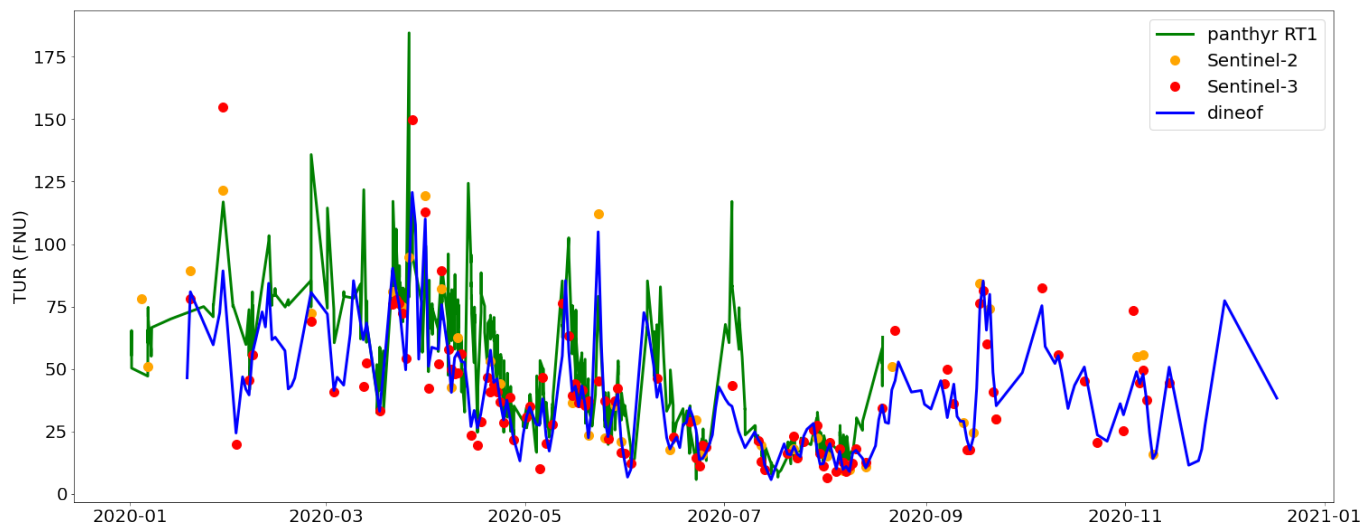
Figure 10. Turbidity time series for 2020 at the RT1 Hypernets station generated using the in situ Hyperspectral Panthyr data (green line), the Sentinel-2 satellite data (orange dots), the Sentinel-3 satellite data (red dots) and the gap-filled DINEOF super resolution satellite product (blue line).
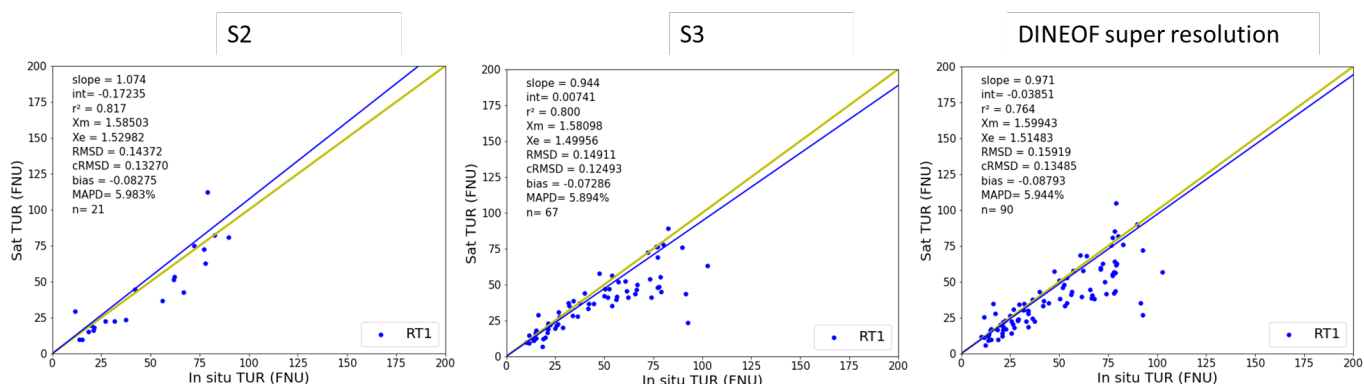
Figure 11. Matchup results of daily Sentinel-2, Sentinel-3 and DINEOF super resolution TUR products against in situ observations obtained from the autonomous PANTHYR system at the RT1 station in the Belgian Coastal Zone.

a full high spatial resolution reconstruction compares with the mixed dataset reconstruction.

345

The DINEOF reconstruction of the mixed dataset used 22 EOFs, and an example of reconstruction is shown in Figure 12. On this date, 1 June 2022, the initial dataset has a spatial resolution of 5 km. A north-south transect shows that the reconstruction (in blue) is able to increase the variability of the 5 km data to mimic the variability of the reference dataset which uses only 1 km resolution data (in green), effectively increasing the spatial resolution of the results with respect to the downgraded dataset,
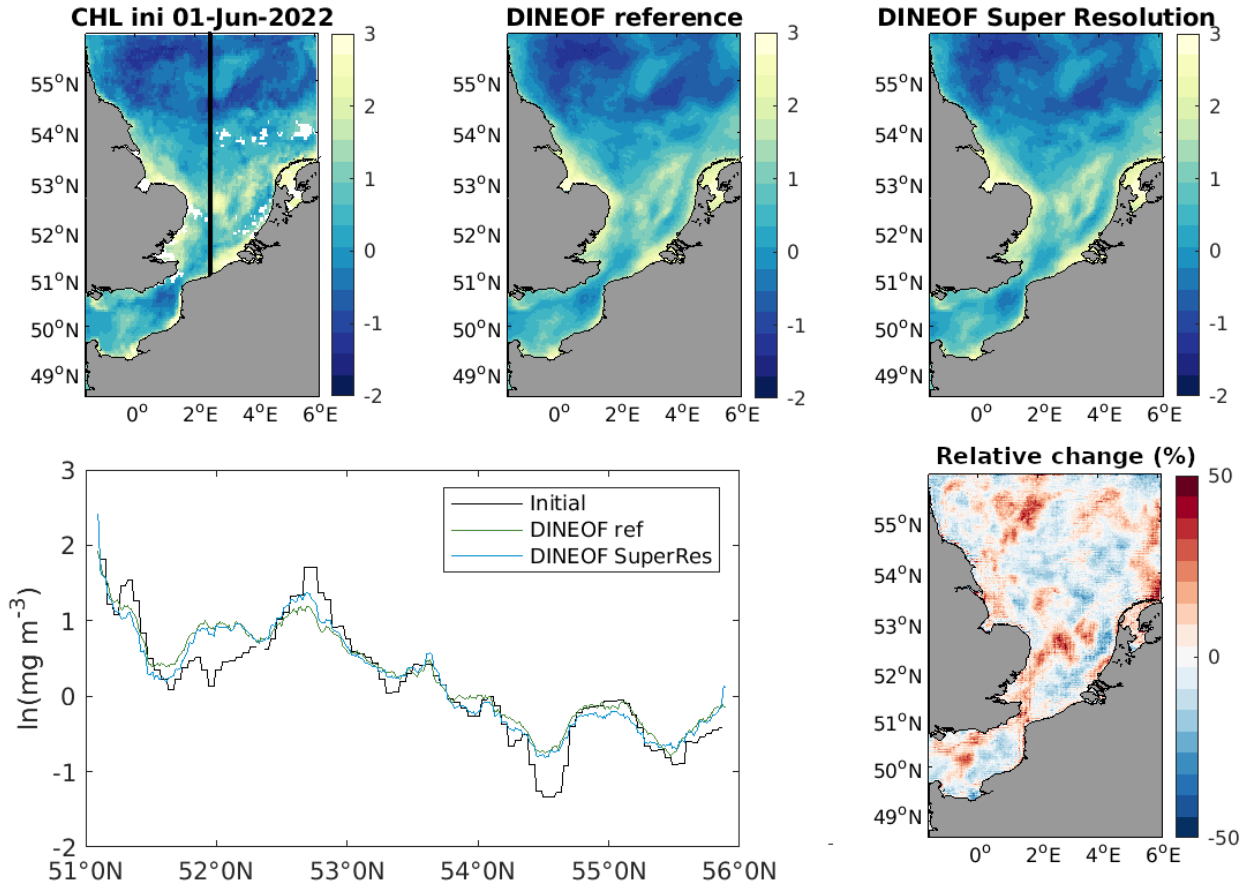
Figure 12. Top left: initially cloudy data with a 1 km resolution, on 1 June 2022. Top center: DINEOF reconstruction of the 5 km data (reference run). Top right: DINEOF run of the mixed dataset. Bottom left: north-south transect for the three datasets (black: initial data at 1 and 5 km; green: reference run at 1km; blue: super-resolution run). Bottom right: percentage difference map between the initial data and the DINEOF estimate. Data in logarithmic scale.

in black, which shows a step-like structure. A percentage difference map is also included, which in addition to showing the regions with higher/lower values in the reconstruction (positive/negative percentage values, respectively), also shows a square pattern that comes from the partial removal of the low resolution information.

In order to investigate this pattern further, figure 13 shows a detail of the reconstruction on 1 June 2022, in which initially 5 km data are present. The super-resolution DINEOF reconstruction (in the right panel of Figure 13) is shown to provide higher spatial resolution than the initial data, similar to what is obtained with the reference reconstruction at 1 km (shown in the central panel of Figure 13), despite the coarse resolution of the initial field. There are some remaining edge effects showing the initial
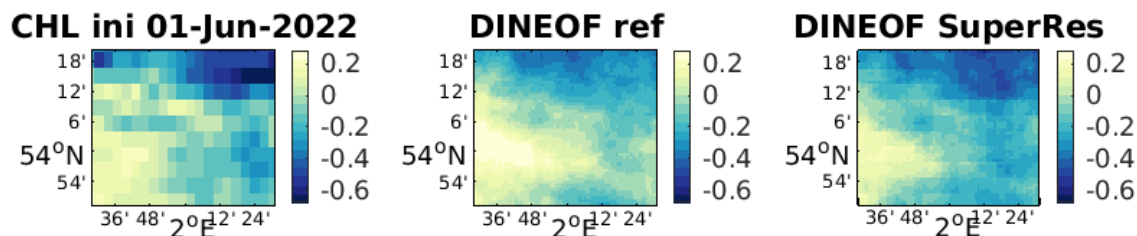
Figure 13. Example of super-resolution DINEOF reconstruction. Left panel: initial data downgraded to 5 km spatial resolution on 1 June 2022. Center panel: reconstruction of the reference run at 1 km spatial resolution. Right panel: reconstruction of the 5 km data with DINEOF using the mixed 1 km and 5 km dataset. Data in logarithmic scale.

5 km grid in the super-resolution, but this comes from the choice of the near-neighbourgh interpolation. A linear interpolation would avoid such pattern in the final results, although this would need to be tested.

On a day with initially 1 km spatial resolution data (figure 14 on 9 July 2022), we can see that the variability observed in the north-south transect for the reference run and the super-resolution reconstruction are very similar, showing the capability of the super-resolution approach to retain small-scale variability.

5 Submesoscale variability in the Belgian Coastal Zone

The super-resolution data obtained in this work allow us to analyse the variability of turbidity at the submesoscale in the study region. The river sediments carried out by the Scheldt and the resuspension of bottom sediments at the along-shore sandbanks are the two major contributors to small-scale variability of turbidity in this region.

Sandbank-induced high turbidity patterns in the Belgian coast are influenced by the topography, and horizontal water movement due to tidal currents results in rapid particle deposition outside of these shallow environments. As a result, turbidity is often high inside the sandbank region and up to about 10 m depth as observed for example in figure 15. We use hourly surface currents obtained from Legrand and Baetens (2021) to assess their influence on turbidity distribution. The intensity of currents and their direction in the hours preceding the time of the satellite pass have a large influence on the average turbidity values over the region, like on 16 October (figure 16) which presents a similar tidal phase than 19 May (top right image) but with
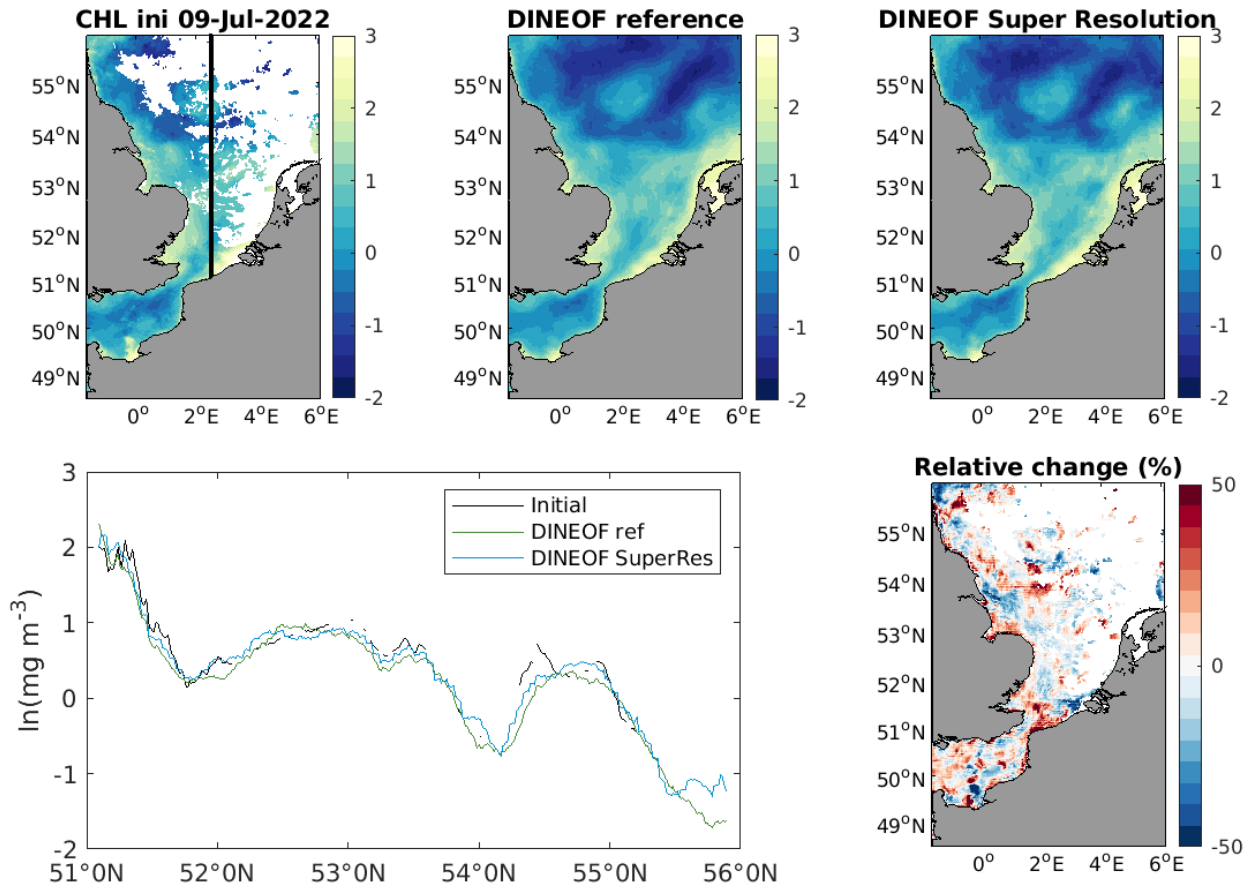
Figure 14. Top left: initially cloudy data with a 5 km resolution, on 9 July 2022. Top center: DINEOF reconstruction of the 1 km data (reference run). Top right: DINEOF run of the mixed dataset. Bottom: north-south transect for the three datasets (black: initial data at 1 and 5 km; green: reference run at 1km; blue: super-resolution run). Bottom right: percentage difference map between the initial data and the DINEOF estimate. Data in logarithmic scale.

stronger currents, resulting on an overall higher turbidity over the whole region.

The bottom panels in figures 15 and 16 show that there is an overall decreasing turbidity in the offshore direction, with similar variability at all depths. The effect of the presence of sandbanks in the resuspension of turbidity is also visible in these images, with regions of higher turbidity corresponding to the presence of these sandbanks. During weak water currents periods (Figure 15), the effect of the sandbanks on water turbidity is clearly seen, with sediments depositing at the deeper, inter-sandbank regions. During strong water current periods (Figure 16), turbidity is higher everywhere, and the effect of the

380

bathymety is less evident.

385 Sandbank-induced high turbidity patterns as in figure 15 are about 2 km wide. Temporal scales of the resuspension-deposition processes are mainly determined by tidal currents. It is therefore not possible to observe these processes with satellite data as they only offer one estimate per day and variations at shorter scales are therefore not measured. Fettweis et al. (2023) showed that in regions with strong tidal regimes, such as in the Belgian coast, the daily sampling from satellites is not enough to capture the variability in the deposition-resuspension cycles caused by tidal currents. Satellite data lack the temporal frequency

390 needed to assess the variability of turbidity at the sandbanks through time, but they provide a relevant tool to analyse the spatial variability at high spatial resolution.

6   Conclusions

There are several satellite datasets monitoring ocean colour globally, but each of those has different spatial, temporal and spectral characteristics. It is therefore necessary to develop approaches that allow to use these data streams in a synergistic way.

395 In the case of coastal studies, there is also a need to work at the highest spatial resolution possible, in order to capture the variability that is typical of these regions. All ocean colour satellite sensors are affected by the presence of clouds, and hence these approaches need to also interpolate missing data.

In this work, we have shown an approach to obtain super-resolution cloud-free satellite data using DINEOF. A combina-

400 tion of Sentinel-2 and Sentinel-3 data representing turbidity in the Belgian coast have been used, and the results show that, working on a combined dataset of Sentinel-2 and Sentinel-3 data, we are able to retain most of the spatial variability present in Sentinel-2 data, and also to increase the spatial variability of the Sentinel-3 data to mimic the Sentinel-2 spatial resolution. The results have been validated using independent in situ data and the ability of DINEOF to increase the spatial resolution has been validated with a chlorophyll dataset covering the whole North Sea. This last example demonstrated that DINEOF is

405 able to recover high spatial resolution information, as compared to the original, high-resolution data that was hidden from the analysis. The approach has been tested in different regions (southern North Sea and Belgian coast in this work) and variables (turbidity and chlorophyll concentration) and can be applied to any other region and variable.

High spatio-temporal resolution data allow to study the small-scale variability in coastal regions, which has been shown

410 in this paper through the influence of sandbanks on turbidity distribution in the Belgian coast. Variables like turbidity or chlorophyll concentration can vary abruptly in a few meters and within a few hours, because of the effect of bathymetry and water currents for example. Using several satellite datasets to analyse these changes allows for a better coverage of the spatio-temporal scales involved. Satellite data lack however the high temporal resolution that would be needed to study the variability of these small-scale features at adequate temporal scales.

415
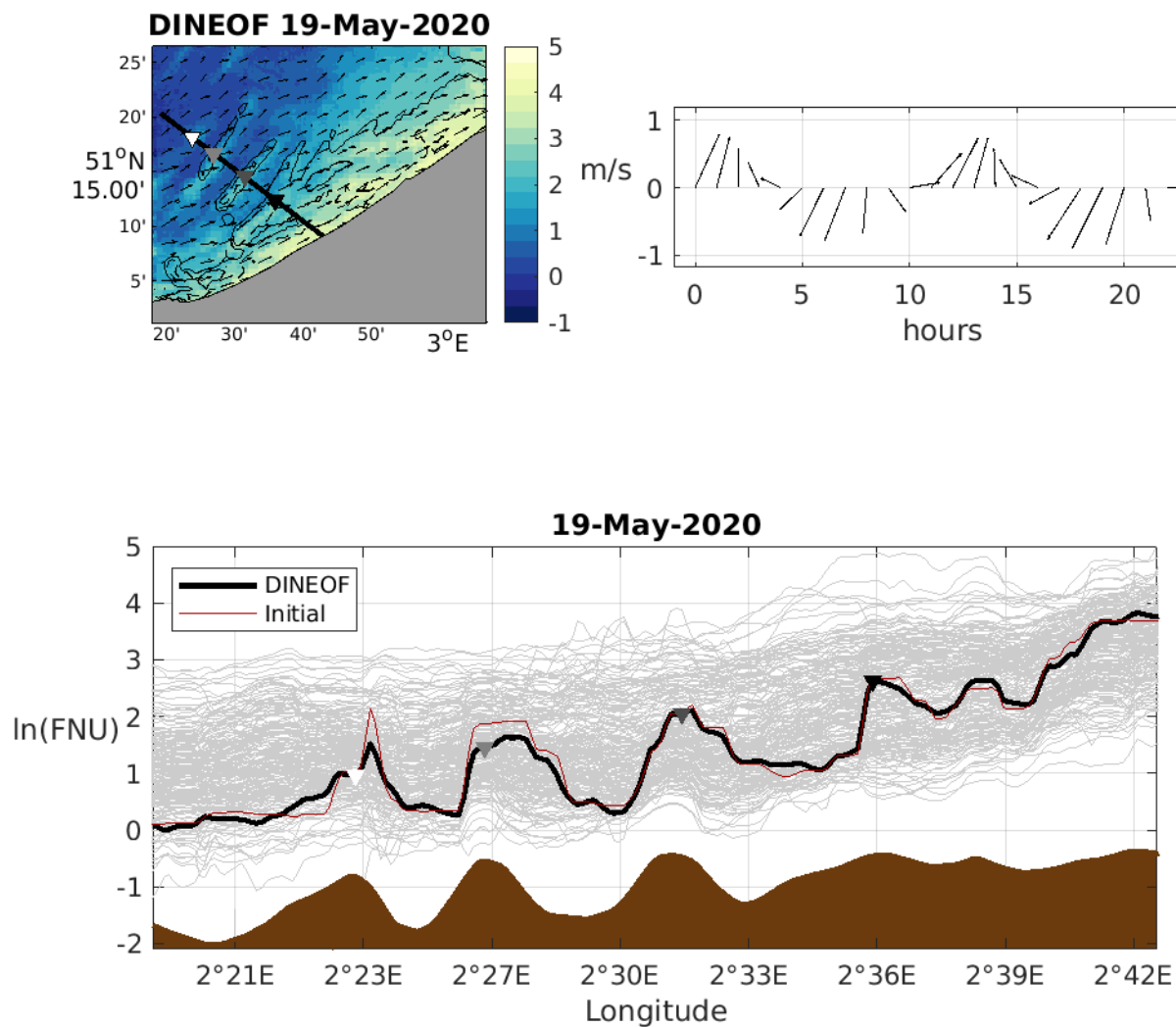
Figure 15. Top left panel: DINEOF super-resolution reconstruction of turbidity on 19 May 2020. Black lines show the 5 m and 10 m isobath and the arrows show surface currents at 10AM. The thick black line shows the transect across sandbanks shown in the bottom panel and the triangles are positioned at the top of some of these sandbanks for reference. Top right panel: hourly surface currents during 19 May at the light grey triangle. Bottom panel: across-sandbank transect of turbidity. Light grey lines show all DINEOF 2020 data, the thick black line shows 19 May turbidity, with the triangles shown to ease comparison with the top left panel. The dark red line shows initial turbidity data and bathymetry is shown in brown.
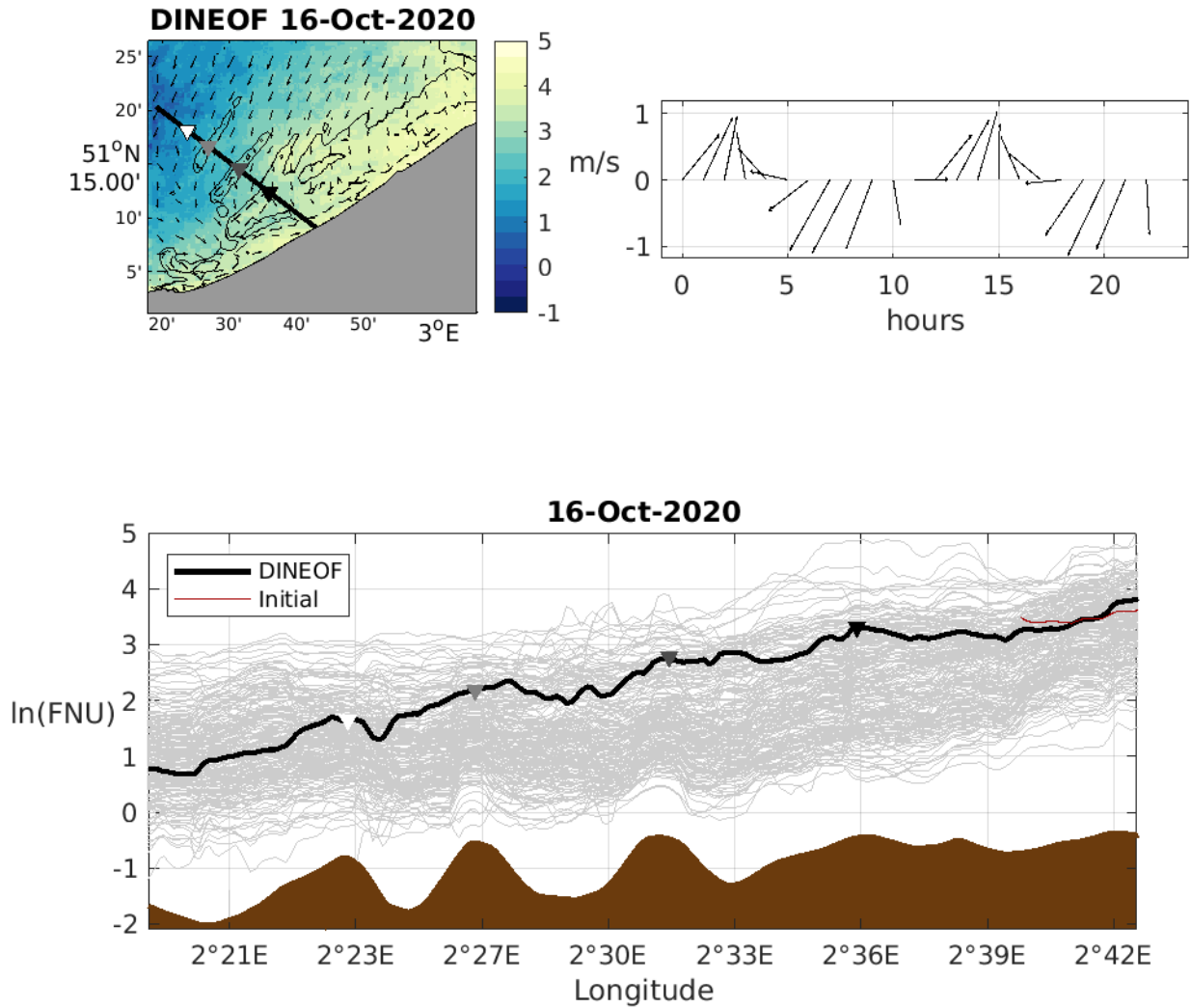
Figure 16. Top left panel: DINEOF super-resolution reconstruction of turbidity on 16 October 2020. Black lines show the 5 m and 10 m isobath and the arrows show surface currents at 10AM. The thick black line shows the transect across sandbanks shown in the bottom panel and the triangles are positioned at the top of some of these sandbanks for reference. Top right panel: hourly surface currents during 16 October at the light grey triangle. Bottom panel: across-sandbank transect of turbidity. Light grey lines show all DINEOF 2020 data, the thick black line shows turbidity on 16 October, with the triangles shown to ease comparison with the top left panel. The dark red line shows initial turbidity data and bathymetry is shown in brown.

Super-resolution satellite products obtained from a synergistic use fo several satellite data streams are necessary to study the coastal ocean. The need for high spatial resolution data decreases at more offshore locations, and therefore the approach presented in this paper could be applied to a multi-resolution dataset with a higher spatial resolution at the most variable regions. Other future developments include the application of the super-resolution DINEOF approach to variables like sea surface tem-
420   perature, although the absence of high spatial resolution data streams with the necessary accuracy makes this a challenge.

Code availability.   DINEOF is available at https://github.com/aida-alvera/DINEOF.

Data availability.   Satellite data used in this work are openly available through the Copernicus Marine Service catalog. This study uses high resolution marine forecast products for the Belgian Coastal Zone as produced by the Royal Belgian Institute of Natural Sciences. The dataset
425   is updated twice a day and can be downloaded at https://erddap.naturalsciences.be/erddap/griddap/BCZ_HydroState_V1.html

Author contributions.   AAA and DVZ designed the study objectives. AAA implemented the super-resolution DINEOF approach and made the reconstructions. DVD, AD and JM prepared the input datasets and made the validation with in situ data. AB and JMB contributed to the DINEOF implementation and the discussions on the experiments. All authors collaborated on the writing.

Competing interests.   At least one of the (co-)authors is a member of the editorial board of Ocean Science.

430   *Acknowledgements.*   This work has been carried out as part of the Copernicus Marine Service MultiRes project. Copernicus Marine Service is implemented by Mercator Ocean in the framework of a delegation agreement with the European Union. The Royal Belgian Institute of Natural Sciences is acknowledged for the ocean currents data.

References

Alvera-Azcárate, A., Barth, A., Rixen, M., and Beckers, J.-M.: Reconstruction of incomplete oceanographic data sets using Empirical Orthogonal Functions. Application to the Adriatic Sea surface temperature., Ocean Modelling., 9, 325–346, https://doi.org/10.1016/j.ocemod.2004.08.001, doi:10.1016/j.ocemod.2004.08.001, 2005.

Alvera-Azcárate, A., Barth, A., Beckers, J.-M., and Weisberg, R. H.: Multivariate Reconstruction of Missing Data in Sea Surface Temperature, Chlorophyll and Wind Satellite Fields, Journal of Geophysical Research, 112, C03 008, doi:10.1029/2006JC003660, 2007.

Alvera-Azcárate, A., Barth, A., Sirjacobs, D., and Beckers, J.-M.: Enhancing temporal correlations in EOF expansions for the reconstruction of missing data using DINEOF, Ocean Science, 5, 475–485, 2009.

Alvera-Azcárate, A., Sirjacobs, D., Barth, A., and Beckers, J.-M.: Outlier detection in satellite data using spatial coherence, Remote Sensing of Environment, 119, 84–91, 2012.

Alvera-Azcárate, A., Vanhellemont, Q., Ruddick, K., Barth, A., and Beckers, J.-M.: Analysis of high frequency geostationary ocean colour data using DINEOF, Estuarine, Coastal and Shelf Science, 159, 28–36, 2015.

Alvera-Azcárate, A., Barth, A., Parard, G., and Beckers, J.-M.: Analysis of SMOS sea surface salinity data using DINEOF, Remote Sensing of Environment, 180, 137–145, 2016.

Alvera-Azcárate, A., der Zande, D. V., Barth, A., dos Santos, J. F. C., Troupin, C., and Beckers, J.-M.: Detection of shadows in high spatial resolution ocean satellite data using DINEOF, Remote Sensing of Environment, 253, 112 229, https://doi.org/https://doi.org/10.1016/j.rse.2020.112229, 2021a.

Alvera-Azcárate, A., der Zande, D. V., Barth, A., Troupin, C., Martin, S., and Beckers, J.-M.: Analysis of 23 Years of Daily Cloud-Free Chlorophyll and Suspended Particulate Matter in the Greater North Sea, Frontiers in Marine Science, 8, https://doi.org/https://doi.org/10.3389/fmars.2021.707632, 2021b.

Bailey, S. and Werdell, P.: A multi-sensor approach for the on-orbit validation of ocean color satellite data products, Remote Sensing of Environment, 102, 12–23, 2006.

Barthélémy, S., Brajard, J., Bertino, L., and Counillon, F.: Super-resolution data assimilation, Ocean Dynamics, 72, 661–678, https://doi.org/https://doi.org/10.1007/s10236-022-01523-x, 2022.

Beckers, J.-M. and Rixen, M.: EOF calculations and data filling from incomplete oceanographic data sets, Journal of Atmospheric and Oceanic Technology, 20, 1839–1856, 2003.

Beckers, J.-M., Barth, A., and Alvera-Azcárate, A.: DINEOF reconstruction of clouded images including error maps. Application to the Sea Surface Temperature around Corsican Island, Ocean Science, 2, 183–199, 2006.

Blondeau-Patissier, D., Gower, J. F., Dekker, A. G., Phinn, S. R., and Brando, V. E.: A review of ocean color remote sensing methods and statistical techniques for the detection, mapping and analysis of phytoplankton blooms in coastal and open oceans, Progress in Oceanography, 123, 123–144, https://doi.org/https://doi.org/10.1016/j.pocean.2013.12.008, 2014.

Buongiorno Nardelli, B., Cavaliere, Davide, D., Charles, E., and Ciani, D.: Super-Resolving Ocean Dynamics from Space with Computer Vision Algorithms, Remote Sensing, 14, https://doi.org/https://doi.org/10.3390/rs14051159, 2022.

Desmit, X., Nohe, A., Borges, A.-V., Prins, T., De Cauwer, K., Lagring, R., Van der Zande, D., and Sabbe, K.: Changes in chlorophyll concentration and phenology in the North Sea in relation to de-eutrophication and sea surface warming, Limnology and Oceanography, 65, 828–847, doi:10.1002/lno.11351, 2020.

Desmit, X., Schartau, M., Riethmüller, R., Terseleer, N., Van der Zande, D., and Fettweis, M.: The transition between coastal and offshore areas in the North Sea unraveled by suspended particle composition, Science of The Total Environment, 915, 169 966, https://doi.org/https://doi.org/10.1016/j.scitotenv.2024.169966, 2024.

Fettweis, M. and Van den Eynde, D.: The mud deposits and the high turbidity in the Belgian–Dutch coastal zone, southern bight of the North Sea, Continental Shelf Research, 23(7), 669–691, https://doi.org/https://doi.org/10.1016/S0278-4343(03)00027-X, 2003.

Fettweis, M., Nechad, B., and den Eynde, D. V.: An estimate of the suspended particulate matter (SPM) transport in the southern North Sea using SeaWiFS images, in situ measurements and numerical model results, Continental Shelf Research, 27, 1568–1583, 2007.

Fettweis, M., Francken, F., Van den Eynde, D., Verwaest, T., Janssens, J., and Van Lancker, V.: Storm influence on SPM concentrations in a coastal turbidity maximum area with high anthropogenic impact (southern North Sea), Continental Shelf Research, 30, 1417–1427, https://doi.org/https://doi.org/10.1016/j.csr.2010.05.001, 2010.

Fettweis, M., Riethmüller, R., Van der Zande, D., and Desmit, X.: Sample based water quality monitoring of coastal seas: How significant is the information loss in patchy time series compared to continuous ones?, Science of The Total Environment, 873, 162 273, https://doi.org/https://doi.org/10.1016/j.scitotenv.2023.162273, 2023.

Groom, S., Sathyendranath, S., Ban, Y., Bernard, S., Brewin, R., Brotas, V., Brockmann, C., Chauhan, P., Choi, J.-K., Chuprin, A., Ciavatta, S., Cipollini, P., Donlon, C., Franz, B., He, X., Hirata, T., Jackson, T., Kampel, M., Krasemann, H., Lavender, S., Pardo-Martinez, S., Mélin, F., Platt, T., Santoleri, R., Skakala, J., Schaeffer, B., Smith, M., Steinmetz, F., Valente, A., and Wang, M.: Satellite Ocean Colour: Current Status and Future Perspective, Frontiers in Marine Science, 6, https://doi.org/10.3389/fmars.2019.00485, 2019.

Kim, J., Kim, T., and Ryu, J.-G.: Multi-source deep data fusion and super-resolution for downscaling sea surface temperature guided by Generative Adversarial Network-based spatiotemporal dependency learning, International Journal of Applied Earth Observation and Geoinformation, 119, 103 312, https://doi.org/https://doi.org/10.1016/j.jag.2023.103312, 2023.

Lacroix, G., Ruddick, K., Gypens, N., and Lancelot, C.: Modelling the relative impact of rivers (Scheldt/Rhine/Seine) and Western Channel waters on the nutrient and diatoms/Phaeocystis distributions in Belgian waters (Southern North Sea), Continental Shelf Research, 27, 1422–1446, https://doi.org/https://doi.org/10.1016/j.csr.2007.01.013, 2007.

Lambhate, D. and Subramani, D. N.: Super-Resolution of Sea Surface Temperature Satellite Images, in: Global Oceans 2020: Singapore – U.S. Gulf Coast, pp. 1–7, https://doi.org/10.1109/IEEECONF38699.2020.9389030, 2020.

Legrand, S. and Baetens, K.: Dataset : Hydrodynamic forecast for the Belgian Coastal Zone, royal Belgian Institute of Natural Sciences, https://metadata.naturalsciences.be/geonetwork/srv/eng/catalog.search#/metadata/BCZ_HydroState_V1, 2021.

Liu, X. and Wang, M.: Super-Resolution of VIIRS-Measured Ocean Color Products Using Deep Convolutional Neural Network, IEEE Transactions on Geoscience and Remote Sensing, 59, 114–127, https://doi.org/10.1109/TGRS.2020.2992912, 2021.

Nechad, B., Ruddick, K. G., and Neukermans, G.: Calibration and validation of a generic multisensor algorithm for mapping of turbidity in coastal waters, vol. 7473, p. 74730H, Proc. of SPIE European International Symposium on Remote Sensing., 2009.

Nechad, B., Ruddick, K., and Park, Y.: Calibration and validation of a generic multisensor algorithm for mapping of total suspended matter in turbid waters, Remote Sensing of Environment, 114, 854 – 866, https://doi.org/https://doi.org/10.1016/j.rse.2009.11.022, 2010.

Nechad, B., Alvera-Azcárate, A., Ruddick, K., and Greenwood, N.: Reconstruction of MODIS total suspended matter time series maps by DINEOF and validation with autonomous platform data, Ocean Dynamics, 61, 1205–1214, doi:10.1007/s10236-011-0425-4, 2011.

Neukermans, G., Ruddick, K., and Greenwood, N.: Diurnal variability of turbidity and light attenuation in the southern North Sea from the SEVIRI geostationary sensor, Remote Sensing of Environment, 124, 564–580, 2012.

Novoa, S., Doxaran, D., Ody, A., Vanhellemont, Q., Lafon, V., Lubac, B., and Gernez, P.: Atmospheric Corrections and Multi-Conditional Algorithm for Multi-Sensor Remote Sensing of Suspended Particulate Matter in Low-to-High Turbidity Levels Coastal Waters, Remote Sensing, 9, https://doi.org/https://doi.org/10.3390/rs9010061, 2017.

Peach, L., Vieira da Silva, G., Cartwright, N., and Strauss, D.: A comparison of process-based and data-driven techniques for downscaling offshore wave forecasts to the nearshore, Ocean Modelling, 182, 102 168, https://doi.org/https://doi.org/10.1016/j.ocemod.2023.102168, 2023.

Ruddick, K. and Lacroix, G.: "Hydrodynamics and meteorology of the Belgian Coastal Zone. Current status of eutrophication in the Belgian Coastal Zone", chap. 1, pp. 1–15, Presses Universitaires de Bruxelles, 2006.

Thiria, S., Sorror, C., T. Archambault, A. C., Bereziat, D., Mejia, C., Molines, J.-M., and Crépon, M.: Downscaling of ocean fields by fusion of heterogeneous observations using Deep Learning algorithms, Ocean Modelling, 182, 102 174, https://doi.org/https://doi.org/10.1016/j.ocemod.2023.102174, 2023.

Van der Zande, D., Vanhellemont, Q., Stelzer, K., Lebreton, C., Dille, A., dos Santos, J., Böttcher, M., Vansteenwegen, D., and Brockmann, C.: Improving operational ocean color coverage using a merged atmospheric correction approach, in: Remote Sensing of the Ocean, Sea Ice, Coastal Waters, and Large Water Regions, edited by SPIE, vol. 12728, pp. 12–29, 2023.

Vanhellemont, Q.: Sensitivity analysis of the dark spectrum fitting atmospheric correction for metre- and decametre-scale satellite imagery using autonomous hyperspectral radiometry, Optics Express, 28, 29 948–29 965, https://doi.org/https://doi.org/10.1364/OE.397456, 2020.

Vansteenwegen, D., Ruddick, K., Cattrijsse, A., Vanhellemont, Q., and Beck, M.: The Pan-and-Tilt Hyperspectral Radiometer System (PANTHYR) for Autonomous Satellite Validation Measurements—Prototype Design and Testing, Remote Sensing, 11, https://doi.org/https://doi.org/10.3390/rs11111360, 2019.

Wilson, R. J. and Heath, M. R.: Increasing turbidity in the North Sea during the 20th century due to changing wave climate, Ocean Science, 15, 1615–1625, https://doi.org/10.5194/os-15-1615-2019, 2019.

Zibordi, G., Mélin, F., Berthon, J.-F., Holben, B., Slutsker, I., Giles, D., D'Alimonte, D., Vandemark, D., Feng, H., Schuster, G., Fabbri, B. E., Kaitala, S., and Seppälä, J.: AERONET-OC: A Network for the Validation of Ocean Color Primary Products, Journal of Atmospheric and Oceanic Technology, 26, 1634 – 1651, https://doi.org/10.1175/2009JTECHO654.1, 2009.

Zou, R., Wei, L., and Guan, L.: Super Resolution of Satellite-Derived Sea Surface Temperature Using a Transformer-Based Model, Remote Sensing, 15, https://doi.org/10.3390/rs15225376, 2023.

Supplementary material

Appendix A: Metrics used in the validation

Estimated dataset mean:

$$\bar{X}^E = \frac{1}{N} \sum_{i=1}^{N} X_i^E \tag{A1}$$
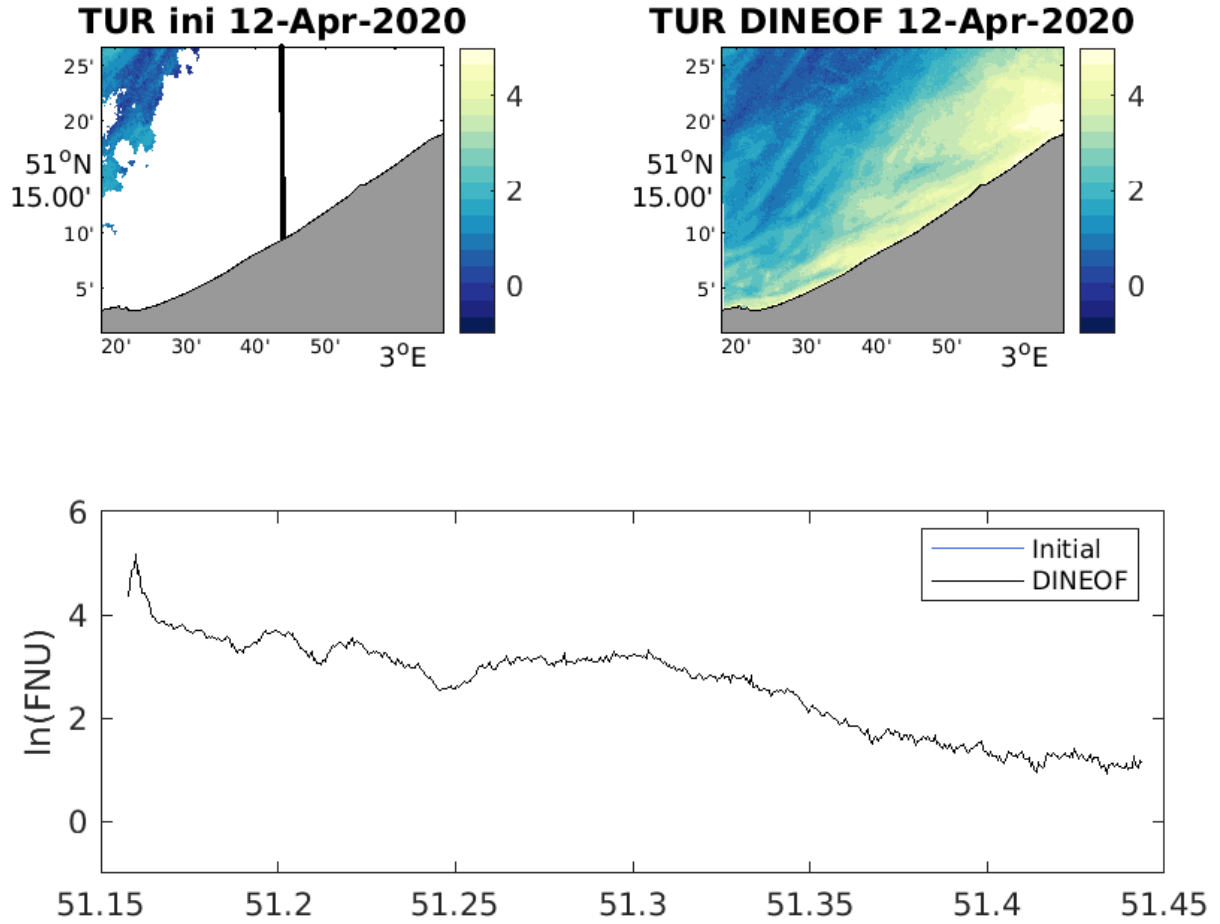
Figure 17. Top left: initially cloudy data at 60 m resolution, on 12 April 2020 (logarithmic scale). Top right: DINEOF run of the mixed Sentinel-2 and Sentinel-3 dataset, at 60 m resolution (logarithmic scale). Bottom: north-south transect for the two datasets (blue: initial data at 60 m; black: super-resolution DINEOF reconstruction). All plots are in logarithmic scale.

Reference dataset mean:

$$\bar{X}^M = \frac{1}{N} \sum_{i=1}^{N} X_i^M \qquad (A2)$$

540
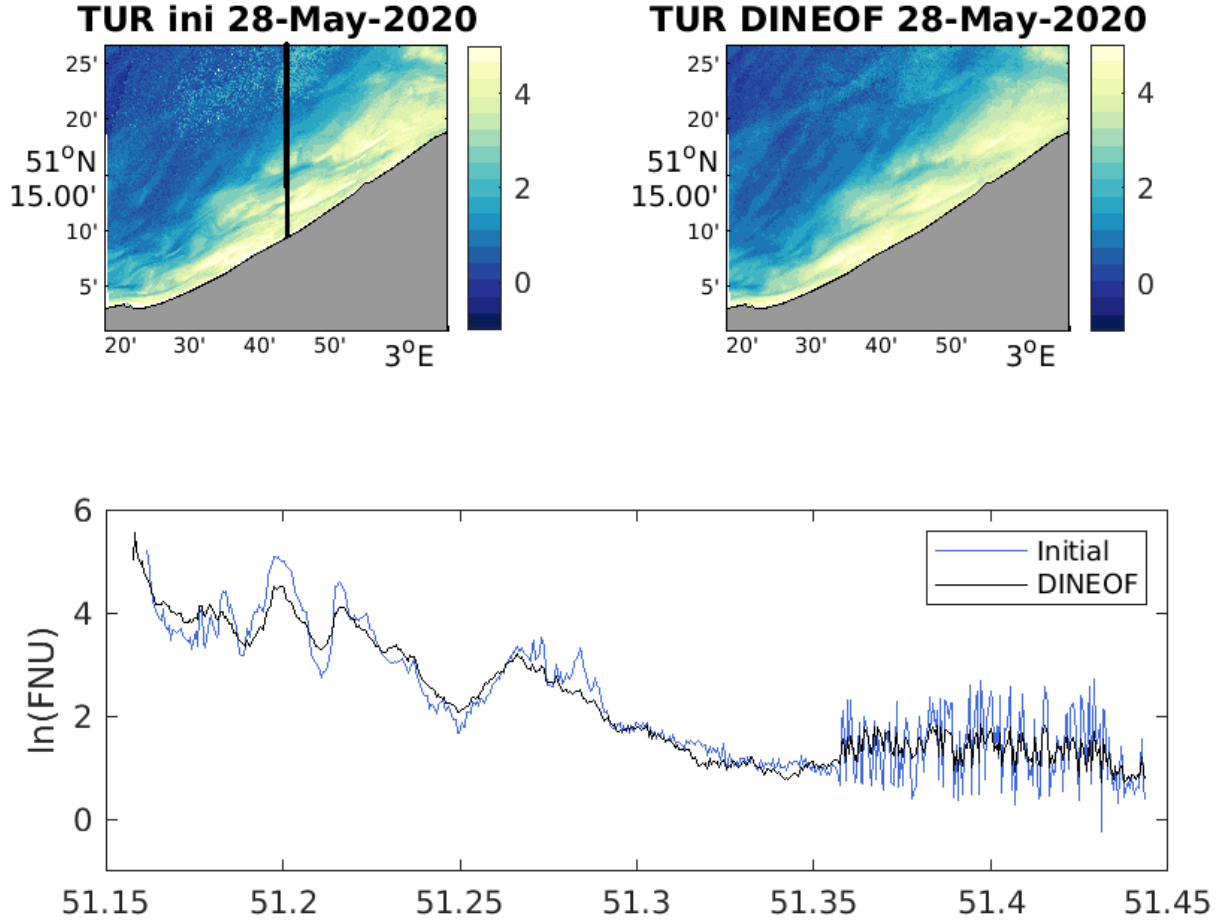
Figure 18. Top left: initially cloudy data at 60 m resolution, on 28 May 2020 (logarithmic scale), with a noisy region in the northern part of the domain. Top right: DINEOF run of the mixed Sentinel-2 and Sentinel-3 dataset (logarithmic scale), at 60 m resolution. Bottom: north-south transect for the two datasets (blue: initial data at 60 m; black: super-resolution DINEOF reconstruction).

Type-2 slope:

$$S = \frac{\sum_{i=1}^{N}\left(Xa^E\right)^2 - \sum_{i=1}^{N}\left(Xa^M\right)^2 + \left[\left(\sum_{i=1}^{N}\left(Xa^E\right)^2 - \sum_{i=1}^{N}\left(Xa^M\right)^2\right)^2 + 4\left(\sum_{i=1}^{N}Xa^E Xa^M\right)^2\right]^{1/2}}{2\sum_{i=1}^{N}Xa^E Xa^M} \tag{A3}$$

with

545 $\quad Xa^E = X_i^E - \bar{X}^E \tag{A4}$

$$Xa^M = X_i^M - \bar{X}^M \tag{A5}$$

Type-2 intercept:

$$I = \bar{X}^E - S\bar{X}^M \tag{A6}$$

Determination coefficient:

$$r^2 = \frac{\left[\sum_{i=1}^{N}\left(Xa^E Xa^M\right)\right]^{1/2}}{\sum_{i=1}^{N}\left(Xa^E\right)^2 \sum_{i=1}^{N}\left(Xa^M\right)^2} \tag{A7}$$

Root Mean Square Difference:

$$\text{RMSD} = \sqrt{\frac{\sum_{i=1}^{N}\left(X_i^E - X_i^M\right)^2}{N}} \tag{A8}$$

Centered Root Mean Square Difference:

$$\text{cRMSD} = \sqrt{\frac{\sum_{i=1}^{N}\left(Xa^E - Xa^M\right)^2}{N}} \tag{A9}$$

Bias:

$$\text{bias} = \frac{1}{N}\sum_{i=1}^{N}\left(Xa^E - Xa^M\right) \tag{A10}$$

Median Absolute Percentage Difference:

$$\text{MAPD} = \text{median}\left(\frac{X_i^E - X_i^M}{X_i^M}\right) \tag{A11}$$